DOI 10.1007/s10778-023-01182-5
International Applied Mechanics, Vol. 58, No. 5, September, 2022

CALCULATION OF DEFLECTIONS DURING BUILD-UP OF SHEET MEMBERS WITH LIQUID METAL

I. K. Senchenkov[1*], I. O. Ryabtsev[2], O. P. Chervinko[1], and A. A. Babinets'[2]**

The current and residual deflections of sheet members during one- and two-layer build-up with three steels under different support conditions are analyzed. A mathematical model of the process is developed. It is based on the theory of built-up bodies, the unified model of viscoplastic flow, and continuous cooling transformation diagrams for microstructural transformations during cooling. The method of numerical modeling of the build-up process based on the finite-element approach is developed. A significant effect of microstructural transformations and support conditions on the residual deflection of surfaced sheet members is established. The correlation between the calculated and experimental data is satisfactory. The obtained results can be used to determine the parameters of the processes of surfacing sheet members.

Keywords: sheet members, multilayered build-up, surfacing, residual deflection, microstructural transformations, unified model of viscoplastic flow, built-up bodies

Introduction. Metal build-up (surfacing) is a process that imparts special properties to the working surfaces of structural members, depending on the operating conditions, such as wear resistance, thermal stability, creep resistance, corrosion resistance, etc. [6, 7].

There are two classes of problems associated with the geometric properties of surfacing objects. The first class includes problems in which the weight of the deposited metal does not exceed several percent of the total weight of the parts. This class includes rolls of rolling mills, rolls of continuous casting machines, NPP reactors, etc.

The second class of problems relates to the modeling of processes during the surfacing of thin-walled members, for example, tubular or sheet members, for which the thickness of the surfaced metal is proportional to the thickness of the parts. The process modeling aim is not only to determine the stress–strain state but also to assess the warping.

Note that when surfacing, especially multilayer thin-walled elements, the thermomechanical fields are strongly dependent on the thickness. Therefore, models that are based on hypotheses for plates and shells have questionable reliability. The results obtained in the framework of a spatial problem statement are more reliable.

The subject of mathematical modeling is the current and residual thermomechanical state of parts during surfacing. The results on this problem are generalized in [3, 6, 7, 17, 18, 21, 22]. A review of the literature allows us to conclude that the surfacing problems of the second class have been studied inadequately.

This paper examines the results of modeling thermomechanical processes during the build-up of prismatic sheet members with rectangular in cross-section made of St3sp steel with one or two layers of liquid steels Sv-08A, Kh18N9T, and 25Kh5FMS using the model of growing bodies [1, 8, 9, 15, 19].

The thermomechanical behavior of materials is described by the Bodner–Partom inelastic flow equation [13, 23]. The microstructural transformations are described using continuous cooling transformation diagrams of austenite decomposition during cooling [10–12]. The problem is solved by the finite-element method [4, 24].

[1]S. P. Timoshenko Institute of Mechanics, National Academy of Sciences of Ukraine, 3 Nesterova St., Kyiv, Ukraine, 03057; *e-mail: term@inmech.kiev.ua. [2]E. O. Paton Electric Welding Institute, National Academy of Sciences of Ukraine, 11 Kazymyra Malevycha St., Kyiv, Ukraine, 03150; **e-mail: ryabtsev39@gmail.com. Translated from Prykladna Mekhanika, Vol. 58, No. 5, pp. 97–108, September–October 2022. Original article submitted November 30, 2021.

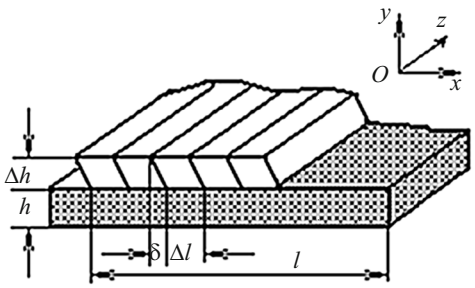

Fig. 1

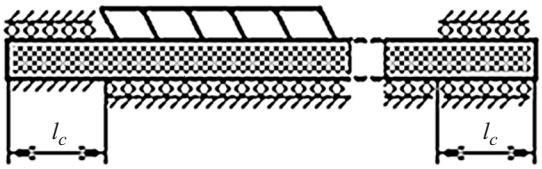

Fig. 2

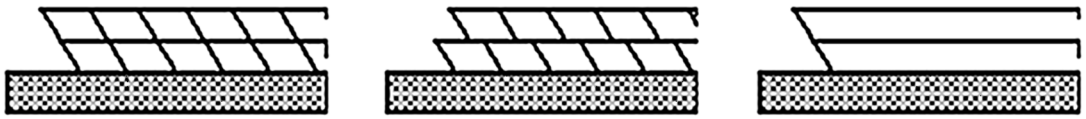

a *b* *c*

Fig. 3

1. Subject of the Research. Consider a sheet (laminated) member made of St3sp steel with rectangular cross-section in the plane *Oxy*. The shape and dimensions of the plate and surfaced rollers are shown in Fig. 1.

Figure 2 schematizes the smooth support of the plate and fixation of sections length l_c of the edges. For comparison, the support scheme with a gap between the plate and the foundation (free support) under the same fixing conditions for the edges is also considered.

To reduce the three-dimensional problem to a two-dimensional one, we use the scheme of simultaneous (instantaneous) build-up of the roller in the direction *Oz*. In this case, the task is to solve either the problem of plane strain state (PSS) or the problem of PSS in the plane *Oxy*, depending on the fixation conditions.

In the case of two-layer surfacing, we consider the schemes of building up the rollers without (Fig. 3*a*) and with (Fig. 3*b*) displacement and a simplified scheme for successive instantaneous build-up of layers (Fig. 3*c*).

2. Model of Microstructural Transformations. In the thermomechanical processes of build-up (surfacing), allotropic transformations in the body due to the decomposition of austenite ($\xi = A$) in steels into the phases of ferrite ($\xi = F$), pearlite ($\xi = P$), bainite ($\xi = B$), and martensite ($\xi = M$) during cooling are taken into account. The transformation of austenite is described by the continuous cooling transformation (CCT) diagram. Figures 4 and 5 show such diagrams for St3sp and 25Kh5FMS steels [10, 11]. The bold lines show the boundaries of the transformation domain, while the thin lines are the cooling curves. The figures near the curves are the volume percentages of austenite decomposition at the exit from the transformation domain.

The law of accumulation of a new phase ξ ($\xi = F, P, B, M$) in the domains along the cooling trajectory is given by the Koistinen–Marburger phenomenological equation [16]:

$$p_\xi = \left[1 - \exp\left(-k\,\frac{\theta_s - \theta}{\theta_s - \theta_e}\right)\right] p_{\xi e},$$

where θ_s, θ_e are the temperatures of the start and end of the transformation; $p_\xi = C_\xi \cdot 100\%$, $p_{\xi e}$ is the maximum value of the new phase for this trajectory; C_ξ is the volume fraction of the phase, $0 \le C_\xi \le 1$, $\sum_\xi C_\xi = 1$, k is the material constant.

The thermomechanical characteristics of each phase Y_ξ are calculated taking into account the temperature dependence $Y_\xi = Y_\xi(\theta)$. The linear mixing rule is used to calculate the macrocharacteristics Y for an arbitrary phase composition. The general formula is

$$\overline{Y}(\theta, t) = \sum_\xi C_\xi(\theta, t) Y_\xi(\theta). \tag{2.1}$$

Physical quantities calculated using the mixing rule can be heat capacity c_V; thermal conductivity k; Young's modulus E; coefficient of linear thermal expansion α; Poisson's ratio ν, and flow model parameters. In Eq. (2.1) and below, the summation

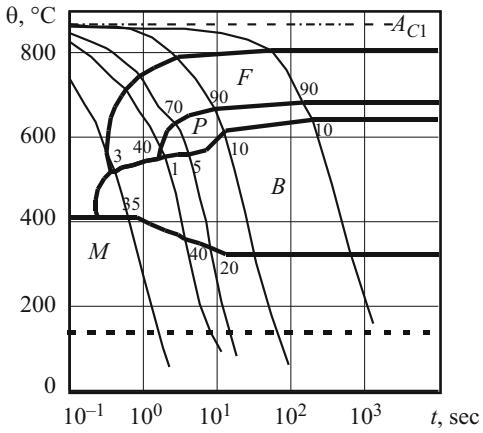

Fig. 4

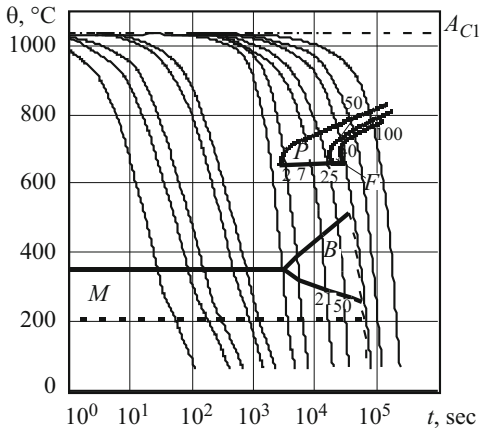

Fig. 5

is over the repeated index. The mixing rule is used over a wide range of temperatures and is in agreement with the experiments in [3, 14, 15, 18].

The thermophase strain $\varepsilon_{ij}^{\theta ph}$ is determined using the specific volumes of the phases V_ξ according to the formula

$$\varepsilon_{ij}^{\theta ph}(\theta, \theta_r, C_\xi) = \frac{V_\xi(\theta)C_\xi(\theta) - V_\xi(\theta_r)C_\xi(\theta_r)}{3V_\xi(\theta_r)C_\xi(\theta_r)}\delta_{ij}. \tag{2.2}$$

Here θ is the current temperature; θ_r is some reference temperature.

The temperature dependence of the specific volumes $V_\xi(\theta)$ for the phase ξ in m^3/kg, at $\theta_r = 20$ °C is taken in the following form [12]:

$$V_\xi(\theta) = V_{\xi_0}[1 + 3\alpha_\xi(\theta - \theta_r)],$$

where α_ξ is the coefficient of linear thermal expansion of the phase ξ; V_{ξ_0} is the specific volume of the phase ξ at the reference temperature.

3. Model of Built-Up Bodies. A feature of the build-up model is that all the components of the stress tensor are specified on the build-up surface [1, 21]. According to Figs. 1–3, the following conditions must be satisfied in the element being built-up:

$$\sigma_{xx} = \sigma_{yy} = \sigma_{zz} = \sigma_{xy} = \sigma_{yz} = \sigma_{xz} = 0 \quad \text{at} \quad t = t^*, \tag{3.1}$$

where t^* is the build-up moment of the roller.

The finite-element method is used to solve the problem. Consider a roller (Fig. 1) built up of liquid metal and attached to a finite-element (FE) mesh. Initially, it has the properties of the "void" material, which is considered thermoelastic and has parameters $E \approx 0, n \approx 0, a = a_f$, where E is Young's modulus; ν is Poisson's ratio; α_f is the coefficient of linear thermal expansion. The thermophysical characteristics of the "void" are assumed to be the same as those of the build-up material.

At the moment t^* of filling the roller, let its empty finite elements $\Delta V(t^*)$ have strain ε_{ij}^* and let it be filled with a material with temperature θ^*.

Thus, conditions (3.1), in fact, mean that when $t = t^*$,

$$\sigma_{ij}(\varepsilon_{ij}^*, \theta^*) = 0 \quad \text{in} \quad \Delta V(t^*). \tag{3.2}$$

It is assumed that the inelastic strain of an element of the layer built up at $t = t^*$ is equal to zero:

$$\varepsilon_{ij}^{p}(t^*)=0 \quad \text{in} \quad \Delta V(t^*). \tag{3.3}$$

In order for the constitutive equations of Hooke's law for the build-up material to be consistent with condition (3.1), it is necessary and sufficient to modify these equations as follows:

$$s_{ij}=2G_f(e_{ij}-\varepsilon_{ij}^{p}-\varepsilon_{ij}^{*}), \qquad \sigma_{ij}=3K_f(\varepsilon_{ij}-\varepsilon_{ij}^{*}-\varepsilon_{ij}^{\theta ph}),$$

$$\varepsilon_{ij}^{p}(t^*)=0, \qquad K_0(t^*)=K_{0f}(\theta^*), \tag{3.4}$$

where s_{ij}, e_{ij} are the deviators of stress and strain tensors; G_f, K_f are the shear and volume compression moduli of the build-up material; K_0 is the isotropic hardening parameter in Eq. (4.2); $\varepsilon_{ij}^{\theta ph}$ is the thermophase strain (2.1); $\varepsilon_{ij}^{\theta ph}(\theta^*)=0$. Here, the subscript f refers to the build-up material. Thus, to satisfy the build-up condition (3.1), all elements that are built up at $t>t^*$ have constitutive equations individualized by those specific values of strain ε_{ij}^{*} and temperature θ^* at which they were filled. Under conditions (3.1), the state $(\varepsilon_{ij}^{*}, \theta^*)$ for these elements can be interpreted as a natural one since it does not cause stresses.

The process of filling elements and the technological parameters of surfacing are detailed in [6, 7].

4. Problem Statement. With the above equations and notation, the mathematical problem statement includes the following equations:

– the equilibrium and thermal conduction equations

$$\sigma_{ij,j}=0, \qquad \bar{c}_v\dot{\theta}=(\bar{k}\theta_{,i})_{,j}+Q \tag{4.1}$$

with the boundary and initial conditions

$$-\bar{k}n_i\theta_{,i}=-q+\gamma(\theta-\theta_C)+\sigma\varepsilon(\theta^4-\theta_0^4), \qquad \theta(0)=\theta_0,$$

– the constitutive equations

$$\varepsilon_{ij}=\varepsilon_{ij}^{e}+\varepsilon_{ij}^{p}+\varepsilon_{ij}^{\theta ph}+\varepsilon_{ij}^{*}, \qquad \varepsilon_{kk}^{p}=0,$$

$$s_{ij}=2G(e_{ij}-\varepsilon_{ij}^{p}-e_{ij}^{\theta ph}+e_{ij}^{*}), \qquad \sigma_{kk}=3K_V(\varepsilon_{kk}-\varepsilon_{kk}^{\theta ph}-\varepsilon_{kk}^{*}).$$

The mechanical boundary conditions are specified as build-up and fixation conditions for an element:

– the flow equation

$$\dot{\varepsilon}_{ij}^{p}=D_0\exp\left\{-\frac{1}{2}\left[\frac{(\bar{K}_0+K)^2}{3s_i}\right]^n\right\}s_{ij}\,/\,s_i, \qquad \varepsilon_{ij}^{p}(0)=0 \tag{4.2}$$

for the main material $\varepsilon_{ij}^{*}(0)=0$

– the evolution equation for the isotropic hardening parameter

$$\dot{K}=m_1(\bar{K}_1-K)\dot{w}_p, \qquad K(0)=0, \tag{4.3}$$

where G, G_f and K_V, K_{Vf} are shear and volume compression moduli; $\bar{K}_0$ and $\bar{K}_1$ are determined by the formulas $\bar{K}_0=C_\xi K_{\xi_0}$, $\bar{K}_1=C_\xi K_{\xi_1}$; C_ξ are the volume concentrations of the phases, $\xi=A, F, P, B, M$, respectively, of austenite, ferrite, pearlite, bainite, and martensite; K_{ξ_0}, K_{ξ_1}, m_1, n, D_0 are the parameters of the model; $\dot{w}_p$ is the plastic strain rate; s_i is the second invariant of the stress tensor; $\dot{w}_p=\sigma_{ij}\dot{\varepsilon}_{ij}^{p}$, $s_i^2=1/2\,s_{ij}s_{ij}$; Q is the heat source; $\bar{k}$ and $\bar{c}_v$ are the averaged coefficients of thermal conductivity and volume heat capacity of the mixture of phases

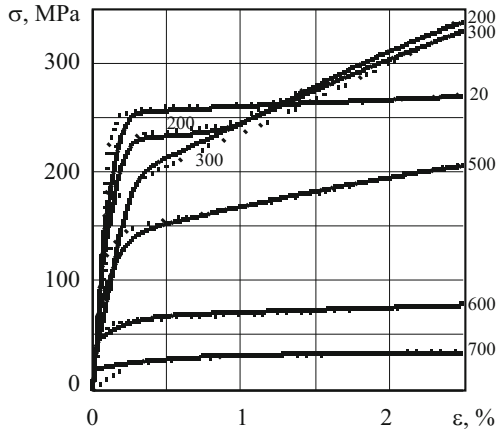

Fig. 6

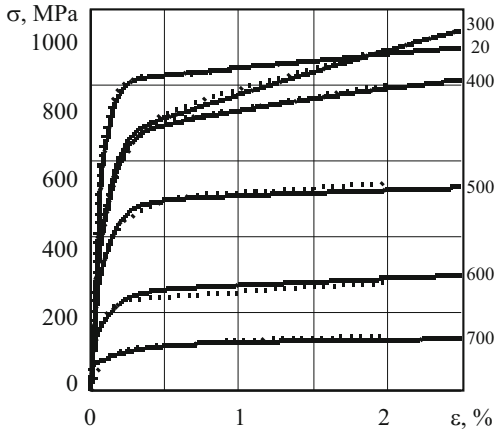

Fig. 7

$$\bar{k} = C_\xi k_\xi, \qquad \bar{c}_v = C_\xi c_{v\xi}.$$

The parameters $\overline{K}_0$ and $\overline{K}_1$ are calculated using the data from [11].

Some materials, such as steels, annealed copper, and aluminum, have significantly flattened initial sections of the tension diagrams. when $m_1 = \text{const}$, the standard Bodner–Partom model provides a too sharp transition from the elastic region to the hardening section. To obtain greater flexibility and better agreement with the test results, Eq. (4.3) should be modified, where the parameter that affects the hardening rate is considered as a function of plastic work or another hardening parameter.

If the parameter m_1 depends on plastic work, we suggest the following evolution equation:

$$\dot{m}_1 = m_{1c}(m_{1b} - m_1)\dot{w}_p, \qquad m_1(0) = m_{1a}, \tag{4.4}$$

where m_{1a}, m_{1b}, m_{1c} are positive constants. Integrating this equation and taking into account the initial condition, we obtain [13]

$$m_1 = m_{1b} + (m_{1a} - m_{1b})\exp(-m_{1c} w_p). \tag{4.5}$$

For materials with so-called temperature-dissimilar tension diagrams, typical of low-carbon steels, Eq. (4.5) is modified as proposed in [20]: the limiting value of the variable hardening coefficient m_{1b} is taken as a function of the inelastic strain that can be represented in the form

$$m_{1b} = m_{1b}^{(2)} + (m_{1b}^{(2)} - m_{1b}^{(1)})\exp\left[-\left(\frac{\varepsilon_{eff}^p}{\varepsilon_0^p}\right)^q\right], \tag{4.6}$$

where $m_{1b}^{(1)}$ and $m_{1b}^{(2)}$ are the initial and limiting values of the parameter m_{1b}; q is the model parameter; ε_{eff}^p is the plastic strain intensity, $\varepsilon_{eff}^p = \sqrt{\frac{2}{3} e_{ij}^p \cdot e_{ij}^p}$; $\varepsilon_0^p(\theta)$ is the plastic strain of transition from the yield plateau to the hardening section of the uniaxial tension diagram (Fig. 6).

5. Thermomechanical Characteristics of the Material. The determination of thermophysical and mechanical characteristics of materials is a rather complex task needed to obtain reliable results. It is important to account for the dependence of these characteristics on temperature and phase composition because they change significantly in the range of change in temperature. The characteristics for the basic phase composition of the materials are presented below. These data are used to determine the characteristics of the model for the current phase composition according to the algorithm presented in [22].

To calculate the parameters of the flow model, we use uniaxial tension diagrams for a constant strain rate. Figures 6 and 7 show tension diagrams from [2, 5] for St3sp and Sv-08A steels at different temperatures and $\dot{\varepsilon} = 5 \cdot 10^{-4}$ sec^{-1}. The dotted and solid lines correspond to experimental and calculated data, respectively. The numbers on the right side of the figures are temperatures in °C.

TABLE 1

θ, °C	$E \cdot 10^{-5}$, MPa	n	m_{1a}, MPa^{-1}	$m_{1b}^{(1)}$, MPa^{-1}	$m_{1b}^{(2)}$, MPa^{-1}	K_0, MPa	K_1, MPa
20	1.98	1.78	0.015	0.015	0.015	685	410
200	1.82	1.305	0.015	0.015	0.18	890	730
300	1.79	1.04	0.14	0.14	0.14	980	1450
350	1.77	0.91	0.13	0.13	0.13	1066	2120
500	1.44	0.85	0.22	0.22	0.22	1210	1050
600	1.14	0.70	1	1	1	719	206
700	0.74	0.5	1	1	1	740	950

TABLE 2

θ, °C	n	m_{1a}, MPa^{-1}	m_{1b}, MPa^{-1}	K_0, MPa	K_1, MPa
20	1.25	5	0.025	540	720
300	0.90	5	0.065	600	1625
400	0.75	7	0.025	1256	1100
500	0.37	10	0.020	7000	8500
600	0.32	10	0.020	9000	9000
700	0.29	10	0.200	9000	9000

The temperature dependences of the Bodner–Partom model parameters for St3sp steel, obtained by processing these diagrams taking into account (4.4), (4.5), are presented in Table 1. The quantities $m_{1c} = 10$, $\varepsilon_0^p = 0.008$, $q = 5$ do not depend on the temperature θ. Hereinafter, $D_0 = 10^4$ sec^{-1}.

The temperature dependences of the flow model parameters for Sv-08A steel, with (4.4) taken into account, are presented in Table 2 ($q = 10$ does not depend on θ).

Figure 8 shows the tension diagrams for 25Kh5FMS steel corresponding to the experimental data beyond the yield point and ultimate strength given in [5]. Figure 9 shows tensile diagrams for Kh18N9T steel [2, 5]. The full circles correspond to the experimental data.

The parameters of the Bodner–Partom model for this steel depending on the temperature, obtained using the standard model (4.3), are presented in Table 3 for $m_1 = 1.4$ MPa^{-1}. Table 4 collects the model parameters for Kh18N9T steel [2, 5].

The temperature dependences of the thermophysical characteristics of materials are taken from [2, 5].

6. Numerical Methods for Solving the Problem. The problem is solved using the methods developed in [4, 6, 7, 20]. The equations with time derivatives are integrated using an implicit scheme with a variable integration step. The nonlinear boundary-value problem of thermomechanics is solved at each step using a simple iteration method and the Steffensen–Aitken convergence acceleration procedure. The linearized problem is solved at each iteration by the finite-element method using a quadrilateral isoparametric element.

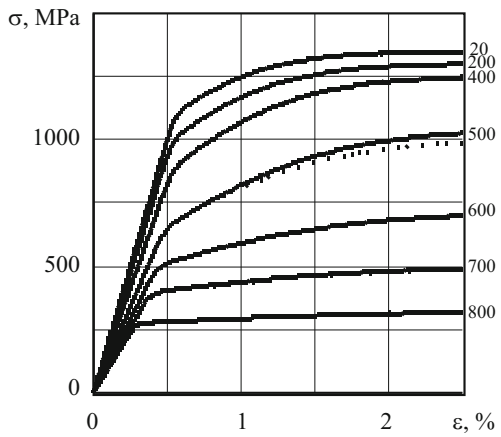

Fig. 8

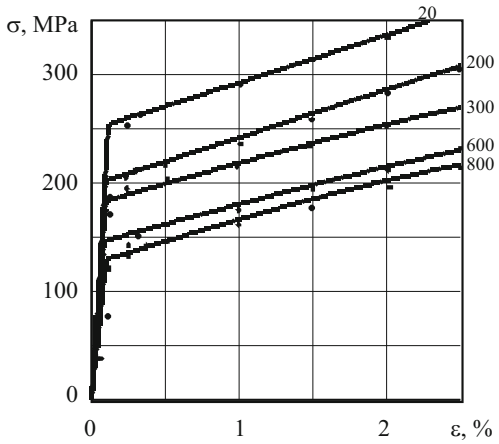

Fig. 9

TABLE 3

θ, °C	n	K_0, MPa	K_1, MPa
20	1.20	4670	1190
100	1.16	4675	1400
200	1.12	4675	1590
300	1.08	4670	1920
400	1.03	4670	2270
500	0.93	4100	2575
600	0.80	4300	2115
700	0.65	5660	2000
800	0.52	7900	200

TABLE 4

θ, °C	n	m_1, MPa^{-1}	K_0, MPa	K_1, MPa
20	1.05	0.043	1360	2100
400	0.93	0.12	1220	1200
0.90	0.155	1050	1190	1190
800	0.85	0.24	1030	1100

7. Calculation of Deflections of Sheet Member during Surfacing. The build-up of the rollers was modeled as schematized in Figs. 1–3.

Input data: $l = 100$ mm, $h = 3$ mm, $\Delta h = 2.3$ mm, $\Delta l = 5$ mm, $l_c = 25$ mm, $l_z = 200$ mm, where l_z is the length of the member along the OZ axis.

The heat transfer coefficient $\gamma = 30$ W/m^2°C for the plate surface and $\gamma = 100$ W/m^2°C for the foundation surface.

The roller and adjacent material strips are preheated during $t_Q = 9$ sec by volumetric heat sources. Their power corresponds to the enthalpy of the melt that is poured in it and to heating by an electric arc to $\theta \approx 1550$ °C.

When this temperature is reached, the actual temperature θ^* and strain ε_{ij}^* of the empty elements of the roller are recorded. Then they are filled with surfacing material whose mechanical properties are described by Eqs. (3.4), (4.2)–(4.5).

After cooling for $t_0 = 23$ sec, surfacing cycles are repeated until the end of the surfacing process. A total of 20 rollers are built up. After cooling, the element is freed from the fastenings shown in Fig. 2, and its residual deflection is measured.

The effect of the martensitic transformation on the kinetics of temperature and displacements is shown at a point in the main material under the 11th roller ($x = 55 \cdot 10^{-3}$ m, $y = 2.5 \cdot 10^{-3}$ m) that is surfaced during $t \in (230–239)$ sec according to Fig. 2

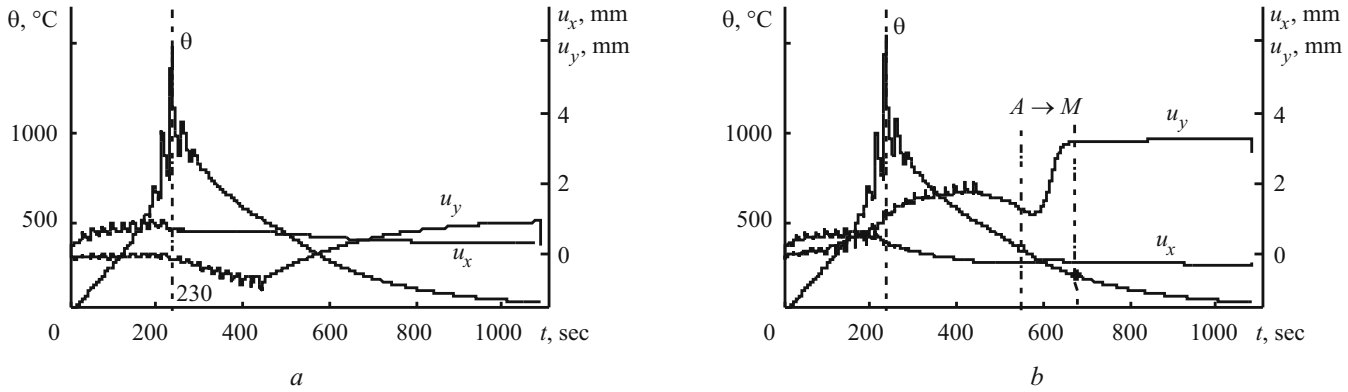

a *b*

Fig. 10

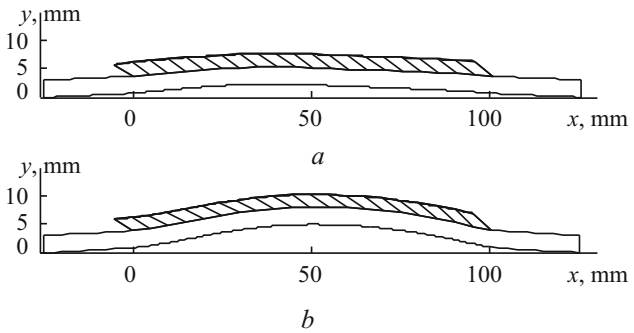

a *b*

Fig. 11

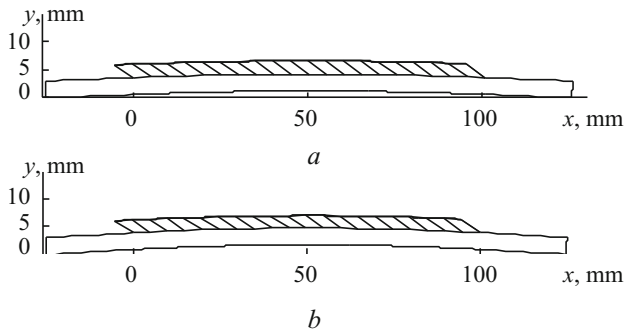

a *b*

Fig. 12

when the lower boundary is free. Such curves are shown in Fig. 10*a* for the case of surfacing with Sv-08A steel and in Fig. 10*b* for surfacing with 25Kh5FMS steel, which undergoes phase transformations during cooling.

In the second case, there is a significant increase in the deflection in the domain of martensitic transformation. The open circles in Fig. 10*b* show the moments of entering and exiting the austenite–martensite transformation domain. The dashed lines bound this domain on the axes θ and t. The instantaneous change in the deflection at $t \approx 1100$ sec corresponds to the release of the right edge of the plate from smooth fixing.

Figures 11*a* and 11*b* compare the residual deflections during roll surfacing (Fig. 2) after releasing the fastening of the ends of the member during surfacing with Sv-08A and 25Kh5FMS steels, respectively, and the free lower boundary.

Figures 12*a* and 12*b* compare the residual deflections for similar problems with smooth support on the lower boundary. Figure 12*a* and 12*b* shows surfacing with Sv-08A steel and 25Kh5FMS steel, respectively.

The deflections in the case of smooth support (Fig. 12) are significantly smaller than in the case of free lower boundary (Fig. 11).

During surfacing with 25Kh5FMS steel in similar load conditions, the deflections are higher (Figs. 11*b* and 12*b*) due to the martensitic transformations, especially in the case of free lower boundary (Fig. 11*b*).

In the case of simultaneous surfacing, we have the following results. Figures 13*a* and 13*b* compare the curves of displacements in the main material at the point ($x = 50 \cdot 10^{-3}$ m, $y = 2.5 \cdot 10^{-3}$ m) for Sv-08A and 25Kh5FMS steels, respectively, in the time interval $t \in 0$–9 sec in the case of free lower boundary. The notation is the same as in Fig. 10.

Although the displacement kinetics differ in the case of phase transformations (Fig. 11*b*), the residual deflections differ insignificantly.

Calculations show that the roll surfacing model predicts larger deflections for both smooth support and free boundary cases compared to the simultaneous surfacing model.

For three surfacing steels Kh18N9T, 2Kh5FMS, and Sv-08A, experimental and calculation data for single-layer surfacing in the cases of smooth support and support with a gap are summarized in Table 5.

Typical deflections were determined as follows. After cooling and freeing the fixed edges, the sample was placed on a smooth plate, and the normal displacement of the upper surface of the plate was measured. The maximum local deflection in the

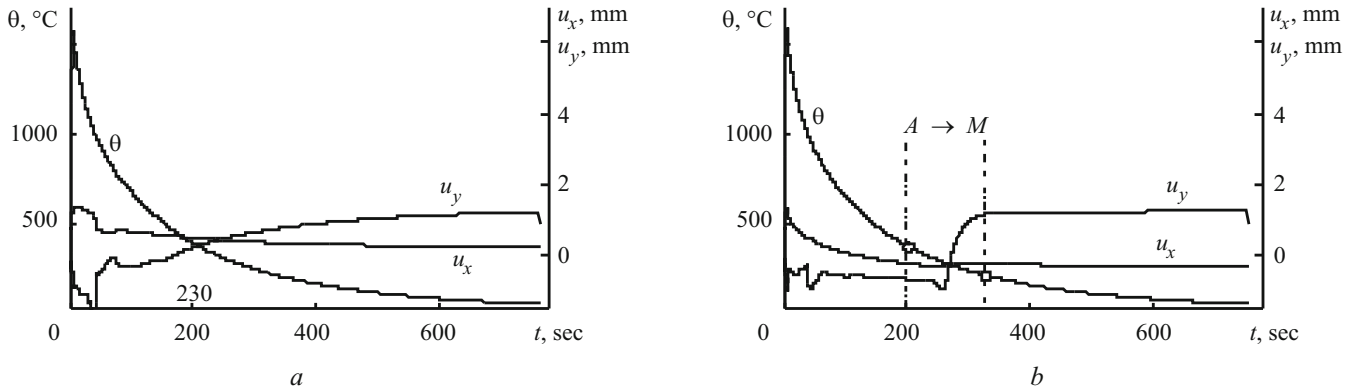

Fig. 13

TABLE 5

Support conditions	Plane strain state/Plane stress state	Materials for surfacing								
		Kh18N9T			25Kh5FMS			Sv-08A		
		Deflections: calculated (1, 2) and experimental (3) data, mm								
		1	2	3	1	2	3	1	2	3
Smooth	Plane strain state	1.45	1.61	0.7	1.52	1.69	1.7	1.21	1.22	0.7
	Plane stress state	1.34	1.38		1.93	1.72		1.13	1.12	
With gap	Plane strain state	2.77	2.18	2.0	2.81	4.96	2.5	2.84	2.27	1.2
	Plane stress state	2.66	1.68		2.55	4.22		2.35	1.69	

cross-section $z = l_z/2$ of the built-up part of the plate was taken as the typical deflection given in this table. This typical deflection is always positive. Columns 1 and 2 contain the calculated data for simultaneous and roll surfacing, respectively. Column 3 contains the experimental data.

Table 5 demonstrates that the deflections in the case of plane strain state are larger than in the case of plane stress state, except for the materials with martensitic transformations (25Kh5FMS). For these materials, larger deflections are due to volumetric transformation effects. Note that during surfacing with a gap between the plate and the welding table, the deflections are larger than when the plate is tightly pressed to the table.

Similar calculations and experiments were carried out for two-layer surfacing. In particular, the following deflections were obtained for Sv-08A steel and smooth support. Schemes without overlap of the rollers (Fig. 3*a*): 1.02 mm in the case of plane strain state and 0.91 mm in the case of plane stress state. The scheme of successive simultaneous surfacing: 1.00 mm in the case of plane strain state and 0.91 mm in the case of plane stress state. The experimental deflection is 0.8 mm. The calculated deflections in the cases of roller surfacing with and without overlap differ by less than 10%.

The disagreement between the calculated and experimental results is due to the inaccuracy of the mathematical model (because of neglecting the contact interaction between the plate and the smooth support) and the technical difficulties in ensuring all the fixation and measurement conditions during the experiments and the number of samples used.

Conclusions. The current and residual deflections of plates made of St3sp steel during build-up using Sv-08A, Kh18N9T, and 25Kh5FMS steels have been calculated in the cases of free boundary and smooth support on the lower surface of the element. In the case of smooth support, the residual deflection is smaller than in the case of free boundary.

During build-up of materials with martensitic transformations, the deflections are larger due to volumetric effects.

In the case of plane strain state, the deflections are larger than in the case of plane stress state, except for the materials with martensitic transformations (25Kh5FMS).

Except for the steel with martensitic transformations (25Kh5FMS), the simultaneous build-up model predicts a larger deflection than the roll build-up model does and can be used to estimate the upper limit of the deflection.

The deflections in two-layer build-up with and without overlap of the rollers in successive layers differ insignificantly.

The calculated results satisfactorily correlate with the experimental data.

REFERENCES

1. N. Kh. Arutyunyan, A. D. Drozdov, and V. E. Naumov, *Mechanics of Growing Viscoelastoplastic Bodies* [in Russian], Nauka, Moscow (1987).
2. N. I. Bezukhov, V. L. Bazhanov, I. I. Gol'denblat, N. A. Nikolaenko, and A. M. Sinyukov, *Strength, Stability, and Vibration Analyses at High Temperatures* [in Russian], Mashinostroenie, Moscow (1965).
3. A. S. Zubchenko (ed.), *Database of Steels and Alloys* [in Russian], 2nd edition, revised and expanded, Mashinostroenie, Moscow (2003).
4. V. I. Makhnenko, *Safe Operation Life of Welded Joints and Components of Modern Structures* [in Russian], Naukova Dumka, Kyiv (2006).
5. I. A. Motovilovets and V. I. Kozlov, *Thermoelasticity*, Vol. 1 of the six-volume series *Mechanics of Coupled Fields in Structural Members* [in Russian], Naukova Dumka, Kyiv (1987).
6. I. A. Ryabtsev and I. K. Senchenkov, *Theory and Practice of Surfacing Operations* [in Russian], Ekotekhnologiya, Kyiv (2013).
7. I. A. Ryabtsev, I. K. Senchenkov, and E. V. Turyk, *Surfacing: Materials, Technologies, Mathematical Simulation* [in Russian], Izd. Silezsk. Politekhn. Inst., Gilwice (2015).
8. I. K. Senchenkov, L. M. Lobanov, O. P. Chervinko, and N. A. Pashchin, "Patterns of relative longitudinal displacements of plates during butt electric welding," *Dop. NAN Ukrainy*, No. 6, 66–70 (1998).
9. I. K. Senchenkov, I. A. Ryabtsev, E. Turyk, and G. A. Tabieva, "Calculation of residual stresses in multilayer spiral surfacing of cylindrical parts based on the theory of build-up of viscous plastic bodies," *Svaroch. Proizv.*, No. 9, 18–25 (2005).
10. A. A. Popov and A. E. Popova, *Isothermal and Continuous Cooling Transformation Diagrams of Supercooled Austenite. Heat-Treater Reference Book* [in Russian], GNTI Mashlit, Moscow–Sverdlovsk (1961).
11. M. Kh. Shorshorov and V. V. Belov, *Phase Transformations and Changes in Steel Properties During Welding. Atlas* [in Russian], Nauka, Moscow (1972).
12. S. F. Yur'ev, *Specific Volumes of Phases in the Martensitic Transformation of Aaustenite* [in Russian], Metallugizdat, Moscow (1950).
13. S. R. Bodner, *Unified Plasticity – an Engineering Approach*, Final Rep. Technion, Israel Inst. Of Tech., Haifa (2000).
14. L. Börjesson and L. E. Lindgren, "Simulation of multipass welding with simultaneous computation of material properties," *ASME, J. Eng. Mater. Tech.*, No. 123, 106–111 (2001).
15. N. W. Klingbeil, J. L. Beuth, R. K. Chin, and C. H. Amon, "Residual stress-induced warping in direct metal solid freeform fabrication," *Int. J. Mech. Sci.*, **44,** No. 1, 57–77 (2002).
16. D. Koistinen and R. Marburger, "A general equation prescribing the extent of the austenite-martensite transformation in pure-carbon alloys and plain carbon steels," *Acta Metallica*, No. **7**, 59–60 (1959).
17. L. E. Lindgren, *Computational Welding Mechanics – Thermomechanical and Microstructural Simulations*, CRC Press, Cambridge (2007).
18. D. Radaj, *Welding Residual Stresses and Distortion. Calculation and Measurement*, DVs Verlag GmbH, Dusseldorf (2003).
19. I. K. Senchenkov, "Thermomechanical model of growing cylindrical bodies made of physically nonlinear materials," *Int. Appl. Mech.*, **41**, No. 9, 1059–1065 (2005).
20. A. Y. Shevchenko, M. V. Banyas, and I. K. Senchenkov, "A variant of the equations of nonisothermal plastic flow," *Int. Appl. Mech.*, **48**, No. 5, 602–607 (2012).

21. I. K. Senchenkov, O. P. Chervinko, M. V. Banyas, “Modelling of thermomechanical process in growing viscoplastic bodies with accounting of microstructural transformations,” in: F. Hetnarski (ed.), *Encyclopedia of Thermal Stresses*, Springer Sci-Disness Media Pordrecht, No. 6, pp. 3147–3157.
22. I. K. Senchenkov and N. D. Oksenchuk, “Modeling of a nonisothermal flow with regard for the dependence of plastic properties on the microstructure of a material,” *J. Math. Sci.*, **190**, No. 6, 796–803 (2013).
23. I. K. Senchenkov and G. A. Tabieva, “Determination of the parameters of the bodner-partom model for thermoplastic deformation of materials,” *Int. Appl. Mech.*, **32**, No. 2, 132–139 (1996).
24. I. K. Senchenkov, G. A. Tabieva, I. A. Ryabtsev, and E. Turyk, “Calculation of residual stresses in multilayer helical surfacing of cylindrical components on the base of the theory of growth of viscoplastic solids,” *Weld. Int.*, **20**, No. 2, 150–156 (2006).